

## A kinetic approach to study the hydrolytic stability of polymer–metal adhesion

A. NAMKANISORN<sup>1</sup>, A. GHATAK<sup>1</sup>, M. K. CHAUDHURY<sup>1,\*</sup>  
and D. H. BERRY<sup>2</sup>

<sup>1</sup> *Department of Chemical Engineering and Polymer Interface Center, Lehigh University, Bethlehem, PA 18015, USA*

<sup>2</sup> *Boeing Commercial Airplanes, Mail Code OM-FM, PO Box 3707, Seattle, WA 98124, USA*

Received in final form 4 June 2001

**Abstract**—A polystyrene–aluminum joint, the adhesion of which was promoted by a silane coupling agent, was examined by fracturing the interface under water at different loads and temperatures. X-ray photoelectron spectroscopy (XPS) analysis of the fractured surfaces showed that the locus of failure was mainly interfacial at low loads, but it gradually moves away from the interface at higher loads. This movement of the failure locus reflects a transition of the mechanism of interfacial debonding from the hydrolysis of the siloxane bonds to the cleavage of the main polymer chains. A rate-dependent bond failure model qualitatively describes the above process, in which the activation energy of bond dissociation is assumed to be a time-dependent parameter.

**Keywords:** Polymer–metal adhesion; fracture energy; aluminum; silane coupling agent; activation energy.

### 1. INTRODUCTION

Polymer–metal joints are used in numerous industries. The advantages of adhesively-coupled polymer–metal junctions over the mechanical methods of assembly, such as riveting and bolting, include reduction of stress concentration near the holes used for mechanical fastening, reduction in weight, and the ability to join thin and/or dissimilar materials [1]. However, one severe shortcoming with polymer–metal joints is the shortening of service life following exposure to water at elevated temperatures. Numerous studies [2–5] document the adverse effects of water on adhesive joints. The locus of failure of well-prepared joints could change from cohesive mode in the adhesive layer to an apparent interfacial mode following

---

\*To whom correspondence should be addressed. Phone: (610) 758-4471. Fax: (610) 758-5057. E-mail: mkc4@lehigh.edu

such exposures. Concomitant with the change in the failure locus, the strength of the joint is also compromised.

The essential requirement for the durability of a polymer–metal joint is the strong interaction between the polymer and the metal surface. The interface must also be resistant to hydrolysis. A variety of techniques [6–16] have been developed to improve the strength and durability of adhesive interfaces. These techniques range from simply degreasing a metal substrate in an alkaline solution to more complex chemical treatments of acid etching and anodization. Each of these pretreatments generates an oxide layer of unique thickness, roughness, topography, and stability. A stable oxide is important as it prevents or minimizes the hydrolysis. Roughness and topography provide an increase in the actual contact area over which interfacial interactions can occur. Therefore, careful selections of the type and quality of surface preparation are important prerequisites for long-term durability of polymer–metal joints.

The strength and durability of joints can also be enhanced using coupling agents [17], which are designed to react with both the organic and its inorganic counterparts. Among various coupling agents, organofunctional silanes are the most common [18]. These silanes effectively combat the water ingress and subsequent hydrolysis by forming a hydrophobic organosilicate layer at the interface. Apart from these chemical approaches, reinforcement of the interface by mechanical interlocking is another useful method to improve strength and long-term durability of adhesive joints.

The fracture of a polymer–metal joint is a complex problem, which involves several molecular interactions and micromechanical processes. The interplay of mechanical deformation in polymer bulk and the strength of the interfacial bond determines the fracture resistance of the joints. Although the interfacial strength is only a small fraction of the measured joint strength, it is a very crucial part [19]. Most of the energy expended to propagate a crack is attributed to the dissipative processes occurring in the bulk of the materials. The general question of how the interfacial processes are coupled to energy dissipative processes is of considerable importance for a fundamental understanding of the molecular and the micromechanical processes that impart the strength and stability to the adhesive joints exposed to various environments.

In this research, we attempted to study the mechanisms involved in the environmental fracture of polymer–metal joints. A model system of a polystyrene block chemically-bonded to a thin film of aluminum was chosen for this purpose, where the extent of bonding between the two materials was controlled by a silane coupling agent. The aluminum film was peeled from polystyrene in water using dead loads at various temperatures. The delamination of the aluminum film from polystyrene occurred slowly in water at loads well below those producing catastrophic failure of the joint. This slow delamination appears to result from the hydrolysis of interfacial siloxane bonds. As the magnitude of the applied load increases, the crack propagation is accompanied by scission of the polystyrene chains. This type of crack growth

exhibits a rate-dependent behavior, which is examined within the framework of interfacial kinetics.

## 2. EXPERIMENTAL

### 2.1. Materials

Aluminum foil (Al 1145 NP, 0.0030 gauge) was purchased from A. J. Oster Co. Styrene monomer (99%) and AIBN initiator, 2,2'-Azobisisobutyronitrile,  $[(\text{CH}_3)_2\text{C}(\text{CN})\text{N}=\text{NC}(\text{CH}_3)_2\text{CN}]$ , were obtained from Aldrich Chemical Co. The silane coupling agent used to improve the interfacial strength of the joint was a styryl functional silane Dow Corning Z<sup>®</sup> 6032,  $\text{CH}_2=\text{CHC}_6\text{H}_4\text{CH}_2\text{NH}(\text{CH}_2)_2\text{NH}(\text{CH}_2)_3\text{Si}(\text{OCH}_3)_3$ . The detergent cleaning of the Al surface was carried out in a sonicator (F35, Fisher Scientific), filled with a 3% aqueous solution of Detergent 8<sup>®</sup> (Alconox, Inc.). The ingredients for chromic-sulfuric acid etching included sodium dichromate dihydrate ( $\text{Na}_2\text{Cr}_2\text{O}_7 \cdot 2\text{H}_2\text{O}$ , Aldrich Chemical Co.) and sulfuric acid (technical grade, Fisher Scientific Co.). The acid for anodization was phosphoric acid (85 wt% solution in water) obtained from Aldrich Chemical Co. A mold for styrene polymerization was cut from a Teflon sheet (TFE, 2.4 mm thick) obtained from McMaster-Carr Supply Co. The microscope used for monitoring the crack propagation was purchased from Optical Apparatus Co., and was equipped with a video camera (Sony, Model XC-75), a video monitor (Sony PVM-97), and a VCR (Sony, Model SVL-390). A translational stage (Melles Griot Co.) was used to fine-control both the vertical and horizontal movements of the sample holder. The hydrothermal peel test was carried out in a 4-l PYREX<sup>®</sup> reaction kettle, enclosed in a heating mantle. An Omega-6100 temperature controller connected to the heating mantle controlled the water temperature in the kettle.

### 2.2. Modification of the aluminum surface

Three methods were used to prepare the aluminum films for the adhesion studies: alkali detergent cleaning, chromic-sulfuric acid etching, and phosphoric acid anodization. The latter two techniques have previously been described by several investigators [7, 10, 11]. Here, only a brief description is given.

*2.2.1. Alkali detergent cleaning.* A 3 wt% solution of Detergent 8<sup>®</sup> (Alconox, Inc.) in water was prepared, and placed in a sonicator. Aluminum foil (3.8 cm × 7.6 cm) was immersed into the solution and sonicated for 30 min, after which it was rinsed copiously with deionized and distilled (DI) water and dried in air. The complete spreading of water on these surfaces served as an indicator of their cleanliness.

*2.2.2. Chromic-sulfuric acid etching.* Aluminum foils (3.8 cm × 7.6 cm) were immersed for 12 min in an aqueous sodium dichromate-sulfuric acid solution

containing sodium dichromate ( $\text{Na}_2\text{Cr}_2\text{O}_7 \cdot 2\text{H}_2\text{O}$ ), sulfuric acid ( $\text{H}_2\text{SO}_4$ ), and water in a 1 : 10 : 30 ratio by weight. The temperature of the etching solution was maintained at  $58^\circ\text{C}$ . At the end of the etching process, the aluminum foils were thoroughly rinsed with DI water and then dried in air.

*2.2.3. Phosphoric acid anodizing.* Aluminum strips ( $3.8\text{ cm} \times 7.6\text{ cm}$ ) were clamped onto a specimen holder and immersed in a 10 wt% phosphoric acid electrolyte at room temperature. A constant anodizing current of 100 mA was then applied to the aluminum for 30 min, after which the aluminum films were rinsed thoroughly with DI water and dried in air.

### *2.3. Preparation of the polystyrene/aluminum joints*

Prior to the polymerization process, styrene monomer was passed through an inhibitor removal column in order to purify the monomer. A reaction mixture was prepared by mixing 24 g styrene monomer, 0.1 g AIBN initiator, and  $5\ \mu\text{l}$  of silane coupling agent ( $\text{Z}^{\text{®}}\ 6032$ ) in a beaker and stirring the mixture thoroughly for 30 min. A rectangular mold ( $3.8\text{ cm} \times 7.6\text{ cm}$ ) of Teflon was clamped to the aluminum foil, and subsequently filled with the reaction mixture. The whole assembly was then placed into a glass Petri dish, and polymerized in an oven at  $75^\circ\text{C}$  for 8 h under nitrogen atmosphere in order to prevent any side reactions of the mixture with the surrounding air. Once the polymerization was completed, the specimen was slowly cooled to room temperature. The next day, the mold was removed and the polystyrene–aluminum joint was recovered for adhesion studies. The polystyrene resulting from the above polymerization scheme has the average molecular weight ( $M_w$ ) of 343 000 and the glass transition temperature ( $T_g$ ) of  $99^\circ\text{C}$  as determined by a dynamic mechanical analyzer (RDA-II, Rheometrics, Inc.). It should be mentioned that although silanes are usually applied onto a substrate by dipping the substrate into a dilute solution of silane or by casting a thin layer of silane on the substrate, we added the silane directly into the monomer solution that polymerized against aluminum. The strength of these joints exhibited superior reproducibility to those obtained by the former methods, perhaps because the amount of silane incorporated into polystyrene could be more accurately controlled. Furthermore, thorough mixing allows better distribution of silane within polystyrene.

### *2.4. Hydrothermal peel test*

The hydrothermal peel test was carried out using the apparatus shown in Fig. 1. After peeling part of the aluminum from the polystyrene in air, a dead load was hung from the free end of the aluminum foil. The entire assembly was immersed in water and rested on a sample support. A thermal jacket, equipped with a temperature controller, was used to maintain the temperature of water. After an induction period, which ranged from 2 to 24 h, the crack propagated at a rate determined

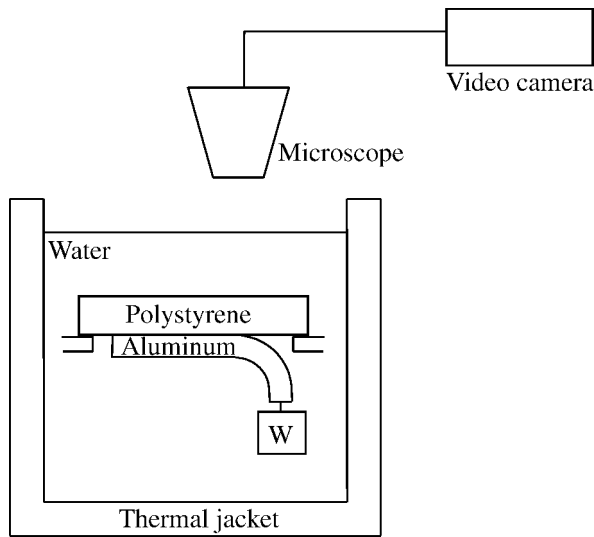


**Figure 1.** A schematic of the experimental apparatus used to study the hydrothermal crack propagation in polystyrene/aluminum joints.

by the applied load, which was monitored and analyzed with a video-microscopic technique.

The fracture energy of the interface ( $G$ ) during the progressive delamination was calculated from the peel force per unit width ( $P$ ) according to the following equation:

$$G = P(1 - \cos \theta), \quad (1)$$

where  $\theta$  is the peel angle, which was fixed at  $90^\circ$  in all these studies. The force acting on the aluminum film was calculated from the dead load corrected for the buoyant forces in water.

### 2.5. Surface analysis

XPS analysis of the aluminum foils before and after delamination was performed on a SCIENTA ESCA-300 instrument. The exciting radiation of this instrument was provided by a monochromatic Al  $K_\alpha$  X-ray source ( $h\nu = 1486.6$  eV) operated at a constant power of 4.5 kW and pass energy of 300 eV. All spectra were taken at a  $90^\circ$  take-off angle. An electron flood gun was used to neutralize the surface charge of the specimen. Data analysis was performed for C 1s, N 1s, O 1s, Si 2p, and Al 2p peaks using SCIENTA's analysis software where the binding energy of each atom was referenced to the binding energy of C 1s (285 eV).

The surface topography of aluminum foils was examined using two techniques: scanning electron (SE) and transmission electron (TE) microscopies. A JOEL-6300 SEM microscope, operating at accelerating voltages of 3–10 kV, was utilized to examine the topography of the oxide layer on aluminum foils. Transmission elec-

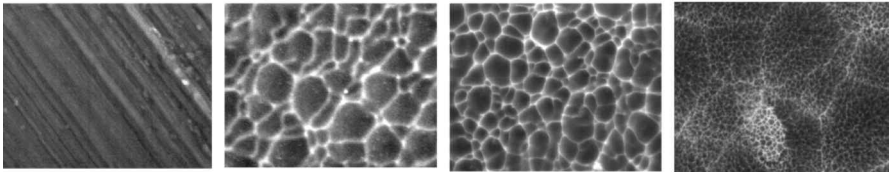
tron microscopy was performed on a Philips-400 transmission electron microscope, operating at the accelerating voltage of 100 kV. The TEM specimens were prepared using an ultramicrotomy technique [20] where very thin sections ( $\sim 40$  nm) of aluminum foil were cut with a  $45^\circ$  diamond knife at room temperature. Once cut, the sections were floated on DI water, and then were collected onto polymer supported grids.

### 3. RESULTS AND DISCUSSION

#### 3.1. Topography of an aluminum surface after pretreatment

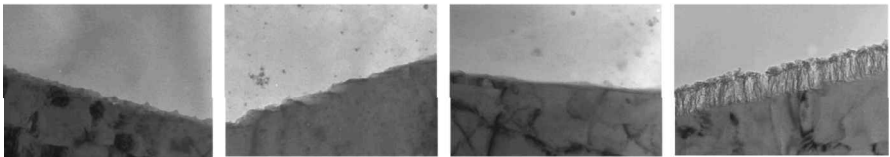
The pretreatment of the aluminum surface serves two main purposes, namely, eliminating the weak oxide layer and then replacing it with a fresh layer of unique surface morphology [9, 12]. SEM micrographs of the aluminum after surface treatment reveal that phosphoric acid anodization produces a finer oxide layer compared to those generated by chromic-sulfuric acid etching, and alkaline detergent cleaning. The latter two treatments, however, produce approximately the same level of surface roughness (Fig. 2). The surface roughness of aluminum was estimated using the atomic force microscopy (AFM), from which the values of root mean square roughness ( $R_{\text{rms}}$ ) of the as-received, detergent cleaned, acid etched and

SEM (top view)



— 200 nm

TEM (cross-sectional view)



— 100 nm

(a) As-received

(b) Sonicated in  
alkaline  
detergent

(c) Chromic sulfuric  
acid etched

(d) Phosphoric acid  
anodized

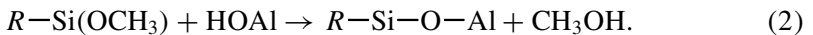
**Figure 2.** SEM and TEM images of the aluminum surface after various treatments.

acid anodized aluminum were 14.2, 20.6, 18.3, and 23.3 nm respectively. These roughness values should, however, be treated as qualitative as they are influenced by the AFM tip shape.

Although the above techniques provide topographic information of the oxide layer generated after treatment, little can be said about its thickness. The investigation of thin sections of the aluminum foils was carried out using a transmission electron microscope (TEM) [13]. TEM micrographs of the metal–oxide zone as shown in Fig. 2 reveal that the thickness of the oxide layers generated by sonication in detergent and acid etching are not significantly different from those of the as-received samples. The thickness of these layers as estimated from TEM micrographs ranges from 5 to 10 nm. In contrast, the oxide layer produced by anodization appears to have a well-organized structure [11, 16, 21]. The oxide layer shows evidence of cracking due to the cutting process. Nevertheless, the oxide layer of about 100 nm in thickness can be distinctly observed.

### 3.2. Mechanism of bonding of polystyrene to aluminum

Styrene monomers were polymerized directly on an aluminum thin film in the presence of a small amount ( $5.3 \times 10^{-3}$ – $2.1 \times 10^{-2}$  mol%) of styryl-functional silane coupling agent (Dow Corning Z<sup>®</sup> 6032) dissolved in the monomer solution. Some of the silanes adsorb on and react with the aluminum surface via its alkoxy group as follows [22]:



The silane modified aluminum film serves to graft polystyrene chains growing in the bulk by a free-radical process. The entanglement of these surface-grafted chains with the bulk matrix provides the strength of adhesion (Fig. 3).

The dry adhesion strength of the above polystyrene film to aluminum is so good that cohesive fracture occurs in polystyrene when an attempt is made to peel the aluminum film from polystyrene. When all the polystyrene homopolymer is removed from the aluminum film by solvent extraction, a thin (10–30 nm) layer of polystyrene remains bonded to aluminum. When another polystyrene film is fused against such an aluminum film, spontaneous adhesion develops. A similar experiment with an unmodified aluminum film produces only weak adhesion. The grafted polystyrene layer on aluminum (i.e. after solvent extraction) is thick enough to screen all the photoelectrons ejected from the aluminum film in the XPS measurements. Ellipsometry was unsuitable to determine the exact thickness of such a grafted layer due to the roughness of the aluminum substrate. However, an equivalent experiment on a polished silicon wafer, which allowed ellipsometric measurements, yielded estimates of the layer thickness ranging from 10 to 35 nm as silane concentration in polystyrene increased from 0.005 to 0.13 mol% (Fig. 4).

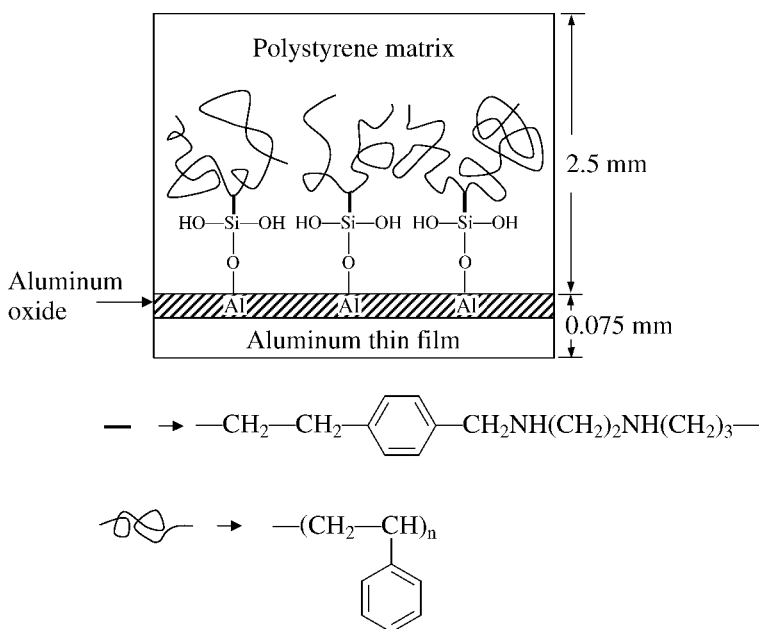


**Figure 3.** Schematic of a polystyrene slab chemically bonded to an aluminum thin film. The silanol groups of the silanes react with the hydroxyl groups of aluminum oxide, whereas its styryl groups serve to graft the polystyrene chains polymerizing in the bulk. The entanglement between the grafted polystyrene chains and those in the matrix results in a strong adhesion of the interface.

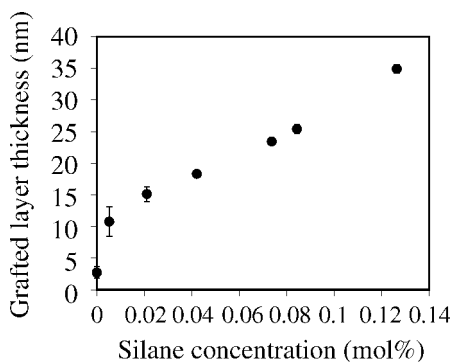


**Figure 4.** Thickness of grafted polystyrene layer remaining on a polished silicon wafer after the homopolymer is removed by solvent (Toluene) extraction. The thickness at zero silane concentration represents the physisorbed layer of polystyrene adsorbed onto silicon wafer. As the amount of silane incorporated in polystyrene increases, the thickness of the surface grafted polystyrene layer increases.

### 3.3. Locus of bond failure

There is a distinct difference between the mode of bond failure when the joint is fractured in air or in water. The optical micrograph of the polystyrene surface after fracture in air reveals features of high surface roughness compared to the rather smooth surface resulting from fracture under water (Fig. 5).

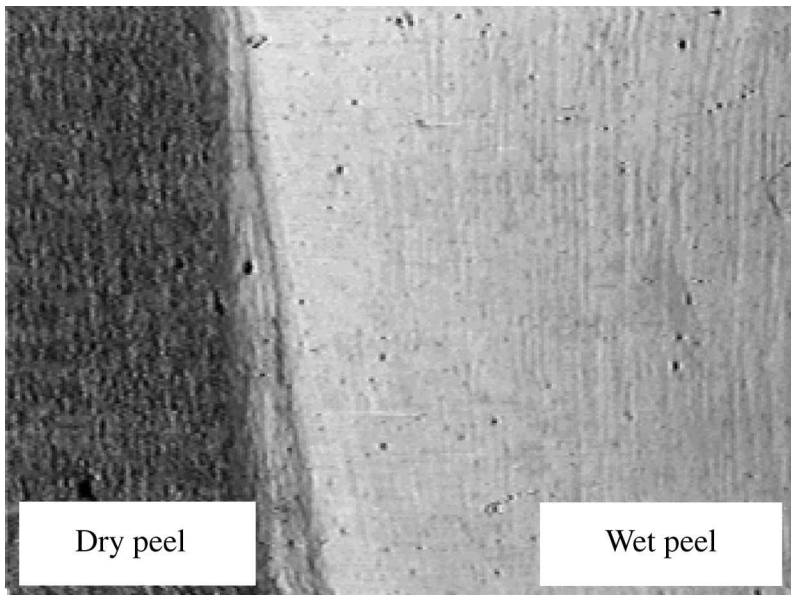


**Figure 5.** Optical micrographs of the fractured polystyrene surfaces showing the transition of failure locus from cohesive mode in polymer bulk to failure close to the interface. Crack propagation under dry peel condition results in the cohesive failure of the polymer as indicated by high surface roughness area (dark contrast), while the near interfacial failure results from peeling under hydrothermal condition (light contrast).

An examination of the aluminum surface after fracture in air reveals the presence of a thin layer of polystyrene on the aluminum foil, indicating that cohesive fracture occurs within the polymer. However, when the joint is fractured under water no film of polymer is visually observed except at high crack propagation speeds. The polystyrene side, on the other hand, exhibited interferometric colors when it was suitably oriented toward a light source. Quantitative analysis of the locus of bond failure was carried out using XPS by determining the elements present on the aluminum foil, which include C 1s, N 1s, O 1s, Si 2p, and Al 2p. The relative composition of carbon (C 1s) and aluminum (Al 2p) are shown in Fig. 6. The initial concentration of carbon present on the aluminum prior to bonding with polystyrene is about 14%. After the aluminum foil is delaminated from polystyrene, the concentration of carbon increases, indicating that some polymer is transferred onto aluminum during delamination. The amount of carbon also increases as the fracture energy ( $G$ ) increases. On the other hand, the concentration of aluminum from Al 2p peak decreases with  $G$ . At the highest value of  $G$ , the aluminum surface is almost completely covered with polymer as indicated by only a small amount of aluminum detected in the XPS spectrum. These results strongly suggest that the crack propagates in very close proximity to the polystyrene–aluminum interface at low values of  $G$ , whereas it deflects away from the interface as  $G$  increases. Since a significant amount of the aluminum is present at intermediate values of  $G$ , it can be

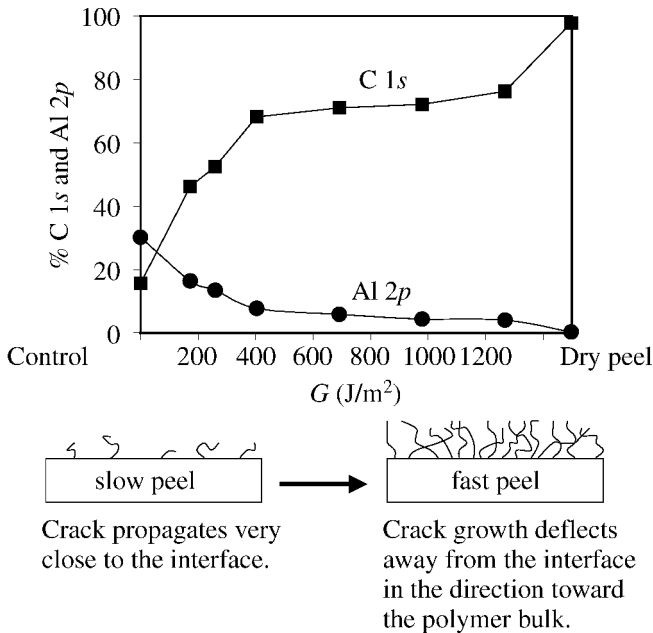


**Figure 6.** The concentration of carbon (C 1s-peak) remaining on the aluminum film after hydrothermal peel tests increases with the fracture energy, while that of aluminum (Al 2p peak) decreases. This indicates that the crack propagates close to the interface at low fracture energy. As the fracture energy increases, the crack locus moves away from the interface toward the bulk of polystyrene. The true cohesive failure is achieved only when the fracture takes place under dry peel condition. In this limit, a complete coverage of aluminum by carbon suggests that the layer of polystyrene left on the aluminum surface is thick enough to shield the aluminum from being detected by the XPS.

inferred that the crack is not entirely in the bulk of the polymer; rather it is restricted very close to the interface. XPS analysis of polystyrene side shows no remnants of aluminum, confirming that the cohesive failure does not occur within the oxide layer present on aluminum.

### 3.4. Mechanism underlying the fracture of polystyrene–aluminum joint

The various processes underlying the fracture of the polystyrene–aluminum joint can be attributed to two primary mechanisms: bond cleavage at or near the interface and an inelastic deformation in the bulk of polystyrene (Fig. 7). The inelastic deformation of aluminum film seems to make a negligible contribution to the overall fracture process (see Appendix).

It is well known that for glassy polymers, the energy required to propagate a crack goes mainly into the growth of a craze at the crack tip. Brown [24] developed a model for the craze-dominated fracture in glassy polymers, according to which the fracture energy is proportional to the square of the interfacial stress ( $\sigma_o$ ), i.e.

$$G = \frac{\sigma_o^2(2\pi D)}{S} \cdot \left(\frac{E_2}{E_1}\right)^{1/2} (1 - 1/\lambda_{\text{craze}}), \quad (3)$$

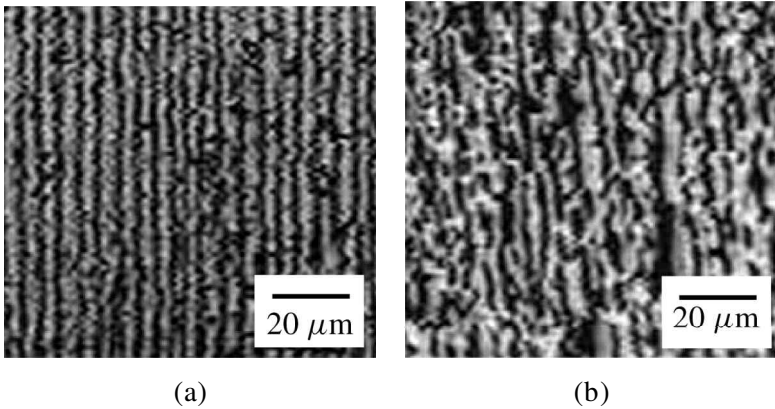


**Figure 7.** Optical micrographs of polystyrene surfaces after hydrothermal peel test indicate that the fracture process is accompanied by a great extent of plastic deformation. (a) and (b) correspond to a low (173 J/m<sup>2</sup>) and high (1120 J/m<sup>2</sup>) fracture energies, respectively. Structures similar to that in Fig. 7a have been reported previously by Xiao *et al.* [23].

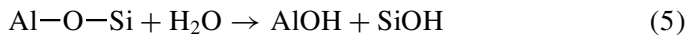
where  $D$  is the diameter of craze fibril,  $\lambda_{\text{craze}}$  is the craze extension ratio,  $S$  is the crazing stress, and  $E_1$  and  $E_2$  are the tensile moduli of the craze in the direction normal and parallel to the craze fibril, respectively. Using the typical literature values of  $S = 55$  MPa,  $\lambda_{\text{craze}} = 3$ ,  $D = 9$  nm, and  $E_1/E_2 = 0.0576$  as obtained from Refs [24] to [26], one finds that the fracture energy ( $G$ ) varies with  $\sigma_0$  as follows:

$$G = 2.86 \times 10^{-15} \cdot \sigma_0^2, \quad (4)$$

where the units of  $G$  and  $\sigma_0$  are J/m<sup>2</sup> and N/m<sup>2</sup>, respectively.

We extend the general features of Brown's model to the polystyrene–metal interface with the understanding that the interfacial stress ( $\sigma_0$ ) is determined by the number of polystyrene chains grafted onto aluminum. The load sustained by each chain, in turn, is determined either by the hydrolysis of the Al–O–Si bond and/or the non-hydrolytic cleavage of the Al–O–Si or C–C bonds, e.g.

(1) hydrolysis of the Al–O–Si bond



(2) non-hydrolytic cleavage of the Al–O–Si bond



(3) cleavage of the C–C bond



When a crack propagates at an extremely slow rate, one expects hydrolysis to be the dominant mechanism of bond cleavage. At fast rate of propagation, non-hydrolytic bond cleavage could dominate the fracture process. Experimentally, it is

found that crack paths at high crack growth velocities shift away from the interface suggesting that the C—C bond breaking becomes the dominant mechanism. The cause of this shift of bond cleavage mode could be that water is not able to reach the interface fast enough to cause hydrolysis or that the internal energy states of the Al—O—Si bond are collimated toward non-hydrolytic cleavage by the external force. In any event, when the Al—O—Si bond ceases to hydrolyze, the fracture path is accompanied with substantial amount of C—C bond cleavage.

At present, however, we do not have a way to opt for either the migration of water or the equilibration of internal states as the mechanism for the change of failure locus. We thus describe this shift empirically by assuming a time-dependent activation energy of the process as follows [27]:

$$E_a(t) = (E_{a1} - E_{a2}) \left(1 - e^{-\frac{t}{\tau}}\right) + E_{a2}, \quad (8)$$

where  $E_{a1}$  is the activation energy of bond hydrolysis,  $E_{a2}$  is the activation energy of non-hydrolytic bond cleavage, and  $\tau$  is the characteristic relaxation time of shifting from one (bond hydrolysis) to the other (bond scission) mode of the fracture process.

The above concept of time dependent activation on bond cleavage, when incorporated into a standard model of thermo-mechanically activated bond dissociation kinetics, allows us to calculate the average time ( $t_{\max}$ ) of survival of a polymer chain adhering to the metal substrate. Since a stress ( $\sigma_o$ ) applied at the interface causes the number of interfacial bonds to steadily decrease with time, the bond breaking process is accelerated due to an increase in the average load sustained by an anchoring site. A detailed kinetic analysis shows that the bonds start failing at a catastrophic rate when a critical time ( $t_{\max}$ ) is reached. The characteristic distance between the bonding sites divided by this critical time allows estimation of the velocity of crack propagation as a function of the interfacial stress ( $\sigma_o$ ). Substitution of this  $\sigma_o$  in equation (4) allows estimation of the total fracture energy ( $G$ ). We thus have a way to calculate how  $G$  varies with the crack propagation velocity ( $V$ ).

### 3.5. Bond dissociation kinetics

According to the kinetic theory of bond dissociation [28], an external force reduces the activation energy of a bond by an amount  $f\lambda$ , where  $f$  is the force acting on the bond and  $\lambda$  is its activation length. The rate of bond dissociation is described as follows:

$$-\frac{d\Sigma}{dt} = k_{\text{off}}\Sigma \exp\left(\frac{f\lambda}{kT}\right), \quad (9)$$

where  $\Sigma$  is the areal density of the bonded sites,  $k$  is the Boltzmann constant, and  $T$  is the absolute temperature. The rate constant of bond breaking ( $k_{\text{off}}$ ) may be expressed as:

$$k_{\text{off}} = \frac{kT}{h} \exp\left(-\frac{E_a(t)}{kT}\right), \quad (10)$$

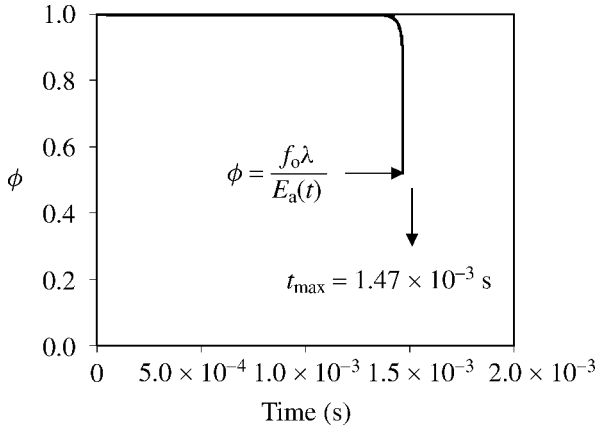


**Figure 8.** The numerical simulation result showing how the density of surface anchoring sites,  $\phi$ , decreases with time when a constant stress ( $\sigma_o = 1.45 \times 10^8 \text{ N/m}^2$ ) is applied at the interface. Here  $\Sigma_o = 1.45 \times 10^{17} / \text{m}^2$ ,  $\tau = 1.0 \times 10^{-3} \text{ s}$ ,  $E_{a1} = 50 \text{ kJ/mol}$ ,  $E_{a2} = 337 \text{ kJ/mol}$ .

where  $h$  is the Planck's constant and  $E_a(t)$  is the time-dependent activation energy of bond dissociation as shown in equation (8). Under a constant applied stress ( $\sigma_o$ ), the number of anchoring sites decreases with time; thus, the force acting on the bond increases according to:

$$f = \sigma_o / \Sigma(t). \quad (11)$$

The rate of dissociation of interfacial bonds is thus expressed as follows:

$$-\frac{d\Sigma}{dt} = \frac{kT}{h} \Sigma \cdot \exp\left(-\frac{E_a(t) - \frac{\sigma_o}{\Sigma} \lambda}{kT}\right). \quad (12)$$

In describing the bond dissociation kinetics, we have neglected the rate at which the bonds are re-formed. This assumption is justifiable for polymers as described in Ref. [32]. Equation (12) can be expressed in terms of a dimensionless parameter  $\phi$ , which is the fraction of chains in the bonded state, i.e.  $\phi = \Sigma / \Sigma_o$ .

$$-\frac{d\phi}{dt} = \frac{kT}{h} \phi \cdot \exp\left(-\frac{E_a(t) - \frac{f_o \lambda}{\phi}}{kT}\right), \quad (13)$$

where  $\Sigma_o$  is the areal chain density of the bonded chains at the interface at  $t = 0$ , and  $f_o = \sigma_o / \Sigma_o$ . The solution of equation (13) gives the distribution of chains as a function of time (Fig. 8).

As shown in Fig. 8,  $\phi$  remains nearly constant as time increases but rapidly decreases after a certain amount of time. When  $f_o \lambda / \phi$  approaches the value of the activation energy  $E_a(t)$ , the barrier of bond dissociation vanishes. The maximum time ( $t_{\max}$ ) of survival of the bond is obtained from the solution of equation (13) by estimating the time taken for  $\phi$  to decrease from unity to  $f_o \lambda / E_a(t)$ . The velocity of crack propagation ( $V$ ) is obtained by dividing the characteristic distance between

the anchoring sites ( $\propto \Sigma_o^{-1/2}$ ) by  $t_{\max}$ , i.e.

$$V = \frac{1}{\sqrt{\Sigma_o} \cdot t_{\max}}. \quad (14)$$

Equation (12), upon which the analysis of crack propagation is based, considers that the crack growth follows a thermally activated process. In order to verify the validity of the above consideration (numerous experiments in other systems [28–33] clearly show this to be true in general), we have conducted peel tests on the polystyrene–aluminum joints under water at different temperatures by applying different amounts of peel loads. The results are summarized in Fig. 9. At each load, the crack velocity increased with temperature following an Arrhenius form (i.e.  $\ln(V) \propto T^{-1}$ ), thus confirming the validity of our assumption, namely, that the crack growth is thermally activated and mechanically assisted [34].

We now examine the relationship between the fracture energy ( $G$ ) and the crack growth velocity ( $V$ ) by solving equations (8) and (13) using the following parameters. The activation energy of bond hydrolysis is taken to be  $\sim 50$  kJ/mol, which is the typical activation energy of the hydrolysis of a siloxane bond [35]. The activation energy of the C–C bond cleavage is taken to be 337 kJ/mol [30]. The bond activation length ( $\lambda$ ) is typically about 0.1 nm, as discussed in Ref. [32]. The adjustable parameters in the simulation are the number density ( $\Sigma_o$ ) of the anchoring sites at the interface and the relaxation time ( $\tau$ ). The value of  $\Sigma_o$  required to describe the experimental results is found to be  $1.45 \times 10^{17}/\text{m}^2$ , which is reasonably close to the values of areal chain density reported in the literature [24, 36].

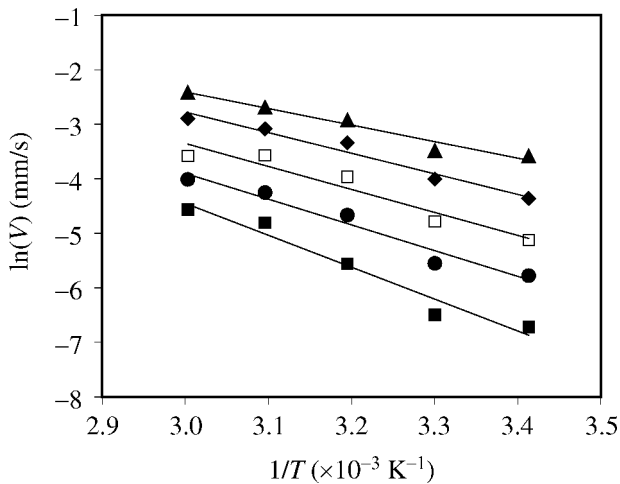
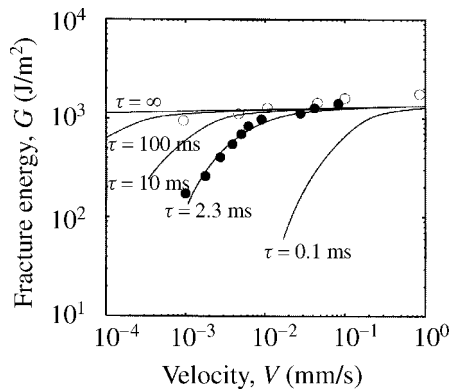


**Figure 9.** The crack growth velocity follows an Arrhenius form. These results were obtained by fracturing a joint of polystyrene containing  $5.3 \times 10^{-3}$  mol% of silane and an acid etched aluminum under water at various temperatures by peeling the aluminum film at different loads. Symbols  $\blacksquare$ ,  $\bullet$ ,  $\square$ ,  $\blacklozenge$  and  $\blacktriangle$  correspond to the fracture energies of 173, 274, 372, 470, and 568 J/m<sup>2</sup>, respectively. Similar behavior is also observed with the detergent cleaned aluminum.

The simulation protocol is as follows. At a given temperature ( $T = 298$  K), the bond survival time ( $t_{\max}$ ) is obtained by estimating the time required for  $\phi$  to decrease from unity to  $f_o\lambda/E_a(t)$  corresponding to a specific value of  $\sigma_o$  (and thus  $f_o$ ). The choice of the value of  $\sigma_o$  allows estimation of  $G$  from equation (4). The corresponding crack growth velocity is obtained from equation (14). The procedures are repeated at different values of  $\tau$  to obtain the  $G$  vs  $V$  curves, which are then compared with the experimental data. Two types of data are analyzed here. In one, the aluminum is peeled from the polystyrene at room temperature in air, which leads to a cohesive failure in the polymer. Fracture energy here is primarily controlled by the scission of the C–C bond, and shows very little dependence on the rate of crack growth velocity. The other set of data is obtained by peeling the joint under water, in which the fracture energy depends significantly on the crack growth rate owing to the transition from bond hydrolysis to cleavage.

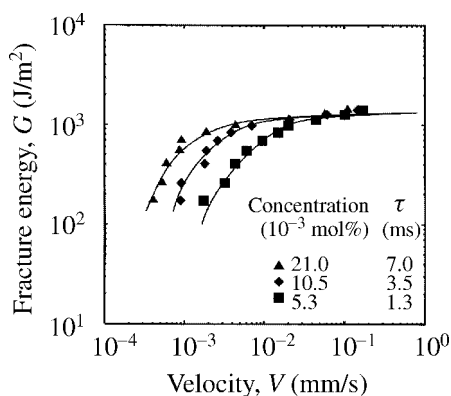
### 3.6. Fracture energy ( $G$ ) as a function of crack propagation velocity ( $V$ )

Figure 10 shows the fracture energies as estimated using equations (13) and (4) and those obtained experimentally. As expected, an increase in the value of  $\tau$  results in the shift of the  $G$ – $V$  curve toward direction of dry peeling ( $\circ$ ). In the absence of hydrolysis, i.e.  $\tau = \infty$ , the simulation corresponds to the peeling under dry condition, whereas the value of  $\tau$  needed to fit the experimental result for hydrothermal peel ( $\bullet$ ) is about 2.3 ms. This is a rather long relaxation time, indicating that  $\tau$  is related, at least partially, to a molecular rearrangement process. This conjecture gains some support from the results obtained with the variation of the coupling agent concentration in polystyrene.



**Figure 10.** Fracture energy ( $G$ ) as a function of crack propagation velocity. Solid lines represent the simulation results (see equation (4));  $\circ$  and  $\bullet$  represent experimental data obtained in dry peel and hydrothermal peel with detergent-cleaned aluminum films, respectively. As the value of  $\tau$  increases, the  $G$ – $V$  curve shifts toward dry peeling.





**Figure 12.** Fracture energy of the interface as a function of crack propagation velocity for various silane concentrations. With a fixed value of  $\Sigma_0 = 1.45 \times 10^{17}$  chains/m<sup>2</sup>, the value of  $\tau$  needed to fit the experimental data increases with the silane concentration.

experimental data, it does not explain why the value of  $\Sigma_0$  should remain the same as the silane concentration increases. Perhaps, a better outlook of the process is as follows. When hydrolysis dominates the fracture process, the interfacial stress is supported by the number of anchoring sites (i.e. Al–O–Si bond) at the interface. This number depends on the concentration of silane as evident from the difference in fracture energy at low crack propagation rates. At higher rates of crack propagation, as the fracture path moves away from the interface, the interfacial stress is supported by the entangled polystyrene chains. This conjecture is consistent with the observation that the fracture energies of the polymer/metal joints all converge to the same value at high crack propagation rates, independent of the silane concentration. This transition from the hydrolysis-controlled interfacial failure to the C–C scission controlled cohesive failure suggests that the initial density of the load bearing sites (i.e.  $\Sigma_0$ ) itself depends on the locus of failure. Proper description of the transition of the failure locus therefore would require, at least, two relaxation schemes — one describing the transition from the bond hydrolysis to bond scission and the other accounting for the transition of the number of load bearing sites. At present, both of these relaxation processes are lumped into one  $\tau$ .

In addition to above complexities, the assumption of first-order kinetics for bond breaking may no longer remain valid for higher silane concentration cases due to the formation of a 2D network, which, in turn, affects the kinetics of bond breaking. Thus, the rate of bond dissociation, as expressed in equation (9), needs to be modified with a suitable order of reaction which has to be determined experimentally.

### 3.8. Effect of surface treatment of aluminum surface

The  $G$ – $V$  curves for various surface treatments of aluminum are compared in Fig. 13. For hydrothermal peeling, the fracture energy,  $G$ , obtained from both the

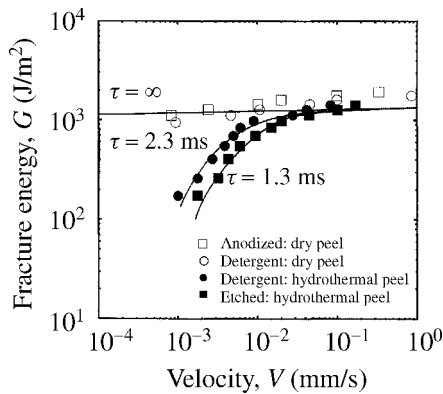


**Figure 13.** Plot of  $G-V$  curves for various cases of surface treatments on aluminum. Open symbols ( $\square$  and  $\circ$ ) represent experimental result obtained by dry peeling, while closed symbols ( $\bullet$  and  $\blacksquare$ ) represent peel results under hydrothermal conditions. The results obtained from numerical simulations are shown as lines with the corresponding values of  $\tau$  needed to fit the experimental data.

detergent cleaned and acid etched surfaces show different values at a given  $V$  in the low velocity range. However, based on the knowledge of the topography of the aluminum surfaces following acid etching and detergent cleaning, one might expect that the difference is small due to a similar nature of the oxide layer present on the aluminum surfaces. The  $G-V$  curves of these two cases are, indeed, not significantly different, the difference being somewhat pronounced in the low velocity range. As the crack growth velocity increases, the fracture energy of both cases merge to the same plateau. The values of  $\tau$  needed to fit the experimental data for these two cases differ roughly by a factor of two, 1.3 ms for etched and 2.3 ms for detergent cleaned surface, respectively. For acid anodized aluminum, whose oxide layer contains well-developed structures of a very fine length scale, the joint does not fracture when it is subjected to similar hydrothermal peel tests. Furthermore, after several days of immersion of the anodized joint, the aluminum corrodes. Thus, for the acid anodized case, the joint could only be fractured under dry condition, which limits the effective mechanism of bond failure to non-hydrolytic bond cleavage. The fracture energy of dry peeling for detergent and acid anodized cases shows very little velocity-dependence, which is in agreement with the results obtained from the numerical calculation in the limit of  $\tau = \infty$ , i.e. in the absence of hydrolysis.

#### 4. CONCLUDING REMARKS

A strong adhesion develops between polystyrene and aluminum when styrene is polymerized onto aluminum in the presence of a silane coupling agent. The same joint weakens considerably when exposed to water. The load and temperature-dependent fracture of these bonds in water follows the Arrhenius behavior as

evident in the linearity between the logarithm of crack growth rate and the inverse temperature. At low loads, fracture locus is very close to the interface whereas it shifts toward the bulk at higher loads. This transition of bond failure locus can be modeled within the framework of interfacial kinetics, in which the activation energy of the process is assumed to be time dependent, reflecting the transition of bond failure mechanism from the hydrolysis of the siloxane bonds to the cleavage of the main polymer chains. Although the model empirically describes the experimental data rather well, the precise origins of the relaxation processes are not well understood. Future studies will be directed toward understanding the detailed nature of the interfacial relaxation processes.

### Acknowledgement

Financial support from the Boeing Company is gratefully acknowledged.

### REFERENCES

1. B. De'Nève and M. E. R. Shanahan, *Polymer* **34**, 5099–5105 (1993).
2. J. K. Jethwa and A. J. Kinloch, *J. Adhesion* **61**, 71–95 (1997).
3. M. R. Bowditch, *Int. J. Adhesion Adhesives* **16**, 73–79 (1996).
4. M. P. Zanni-Deffarges and M. E. R. Shanahan, *Int. J. Adhesion Adhesives* **15**, 137–142 (1995).
5. H. M. Clearfield, D. K. McNamara and G. D. Davis, in: *Adhesive Bonding*, L. H. Lee (Ed.), pp. 205–212. Plenum Press, New York (1991).
6. K. B. Armstrong, *Int. J. Adhesion Adhesives* **17**, 89–105 (1997).
7. G. W. Critchlow and D. M. Brewis, *Int. J. Adhesion Adhesives* **16**, 255–275 (1996).
8. R. P. Digby and D. E. Packham, *Int. J. Adhesion Adhesives* **15**, 61 (1995).
9. J. A. Marceau, *SAMPE Q.* **9**, 1–7 (1978).
10. A. V. Pocius, *J. Adhesion* **39**, 101–121 (1992).
11. J. D. Venables, *J. Mater. Sci.* **19**, 2431–2453 (1984).
12. D. J. Arrowsmith and A. W. Clifford, *Int. J. Adhesion Adhesives* **3**, 193–196 (1983).
13. E. A. Ledbury, A. G. Miller, P. D. Peters, E. E. Peterson and B. W. Smith, in: *Proc. 12th Nat. SAMPE Tech. Conf.*, pp. 935–950 (1980).
14. G. E. Thompson, *Thin Solid Films* **297**, 192–201 (1997).
15. J. D. Venables, D. K. McNamara, J. M. Chen, T. S. Sun and R. L. Hopping, *Appl. Surface Sci.* **3**, 88–98 (1979).
16. W. Brockmann, O.-D. Hennemann, H. Kollek and C. Matz, *Int. J. Adhesion Adhesives* **6**, 115–143 (1986).
17. P. G. Pape and E. P. Plueddemann, in: *Proc. Soc. Plastics Engineers ANTEC*, pp. 1870–1875 (1991).
18. K. L. Mittal (Ed.), *Silanes and Other Coupling Agents*, Vol. 2. VSP, Utrecht, The Netherlands (2000).
19. G. D. Davis, *Mater. Res. Soc. Symp. Proc.* **304**, 3–13 (1993).
20. K. Shimizu, G. M. Brown, K. Kobayashi, P. Skeldon, G. E. Thompson and G. C. Wood, *Corrosion Sci.* **40**, 1049–1072 (1998).
21. G. M. Brown, K. Shimizu, K. Kobayashi, P. Skeldon, G. E. Thompson and G. C. Wood, *Corrosion Sci.* **40**, 1575–1586 (1998).
22. E. P. Plueddemann, *Silane Coupling Agents*. Plenum Press, New York (1982).
23. F. Xiao, C. Y. Hui, J. Washiyama and E. J. Kramer, *Macromolecules* **27**, 4382–4390 (1994).

24. H. R. Brown, *Macromolecules* **24**, 2752–2756 (1991).
25. C.-A. Dai, E. J. Kramer, J. Washiyama and C.-Y. Hui, *Macromolecules* **29**, 7536–7543 (1996).
26. L. L. Berger, *Macromolecules* **22**, 3162–3167 (1989).
27. Note that a similar time dependent activation process has been used by M. Karplus, *J. Phys. Chem. B* **104**, 11–27 (2000) to describe the complex behavior of protein reaction, specifically, ligand binding by myoglobin.
28. A. Tobolsky, R. E. Powell and H. Eyring, in: *Chemistry of Large Molecules*, R. E. Burk and O. Grummitt (Eds). Interscience Publishers, New York (1943).
29. A. Schallamach, *Wear* **6**, 375 (1963).
30. H. H. Kausch, in: *Polymer Fracture*, Vol. 2, pp. 53–86. Springer-Verlag, Berlin (1987).
31. A. S. Krausz and K. Krausz, in: *Fracture Kinetics of Crack Growth*, Vol. 1, pp. 23–94. Kluwer Academic Publishers, Dordrecht, The Netherlands (1988).
32. M. K. Chaudhury, *J. Phys. Chem. B* **103**, 6562–6566 (1999).
33. A. Ghatak, K. Vorvolakos, H. She, D. Malotky and M. K. Chaudhury, *J. Phys. Chem. B* **104**, 4018–4030 (2000).
34. N. Shephard and J. P. Wightman have found that the crack growth follows a similar activation process in silicone rubber bonded to metal oxides as well (N. Shephard, personal communication).
35. G. Leturcq, G. Berger, T. Advocat, C. Fillet, O. Halgand and E. Vernaz, *Mater. Res. Soc. Symp. Proc.* **506**, 199–206 (1998).
36. M. Sambasivam, A. Klein and L. H. Sperling, *Macromolecules* **28**, 152 (1995).
37. A. N. Gent and G. R. Hamed, *J. Appl. Polym. Sci.* **21**, 2817–2830 (1977).

## APPENDIX

### *Estimation of the energy contributed to plastic yielding of an aluminum strip*

Even though the energy of plastic deformation in the polymer constitutes a large portion of the fracture energy of the interface, a small, albeit negligible, contribution to plastic yielding arises due to the deformation of aluminum strip. The contribution of plastic yielding of the aluminum strip to the fracture energy was estimated using Gent's method [37]. For a 90° peel test (Fig. A1), the energy contributed to plastic yielding of aluminum strip can be expressed as:

$$P_y = \frac{\sigma_y T_s^2}{4R}, \quad (\text{A1})$$

where  $P_y$  is the energy contribution due to plastic yielding on aluminum strip,  $\sigma_y$  is the yield stress of the aluminum foil ( $1.77 \times 10^8 \text{ N/m}^2$ ),  $T_s$  is the foil thickness, and  $R$  is the radius of curvature of the aluminum strip being peeled, which is inversely proportional to the peel load.

The energy contribution of plastic yielding in the aluminum strip was determined by measuring the radius of curvature of aluminum strip at the end of the peel test after allowing its elastic recovery, and calculating the value of  $P_y$  according to equation (A1). Although most of the peel tests in our study were done under hydrothermal condition, the estimation for the dry peel case represents the upper limit of  $P_y$  as the aluminum strips under dry peel condition bend more severely than

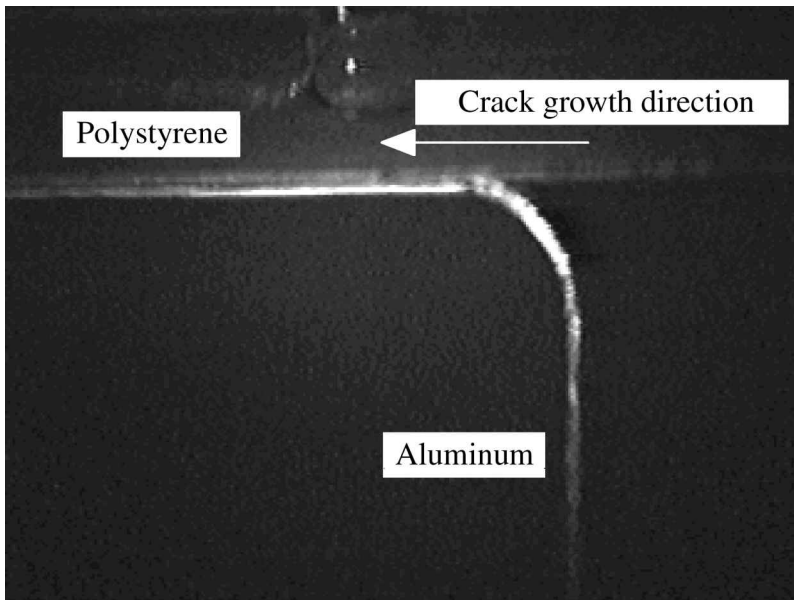


**Figure A1.** An experimental setup for the estimation of the energy contributed to plastic yielding of aluminum strip.

**Table A1.**

The contribution of energy arising from plastic yielding of aluminum strip to the fracture energy as determined by equation (A1)

Fracture energy ( $J/m^2$ )	Energy contributed by plastic yielding of aluminum, $P_y$ ( $J/m^2$ )	% of energy contributed by plastic yielding of aluminum
1111	15.9	1.4
1437	17.4	1.2
1764	22.4	1.3

those peeled under water. As shown in Table A1, an insignificant fraction of the fracture energy (1.2–1.4%) is contributed by the plastic yielding in the aluminum strip.